Analysis of the Role of the Interleukin-2 Receptor γ Chain in Ligand Binding[†]

Stefano F. Liparoto,[‡] David G. Myszka,[§] Zining Wu,[||] Byron Goldstein,[⊥] Thomas M. Laue,[#] and Thomas L. Ciardelli*,[△,▽]

Department of Biological Chemistry, The University of Michigan Medical School, Medical Sciences Building I, Ann Arbor, Michigan 48109-4581, Center for Biomolecular Interaction Analysis, University of Utah, Salt Lake City, Utah 84132, Department of Protein Biochemistry, GlaxoSmithKline Pharmaceuticals, 709 Swedeland Road, UE0430, P.O. Box 1539, King of Prussia, Pennsylvania 19406-0939, Theoretical Biology and Biophysics, Los Alamos National Laboratory, Los Alamos, New Mexico 87545, Department of Biochemistry and Molecular Biology, University of New Hampshire, Durham, New Hampshire 03867, Research Service, Veterans Administrations Hospital, White River Junction, Vermont 05009, and Department of Pharmacology and Toxicology, Dartmouth Medical School, Hanover, New Hampshire 03755

Received August 21, 2001; Revised Manuscript Received November 14, 2001

ABSTRACT: Interleukin-2 is the primary T cell growth factor secreted by activated T cells. IL-2 is an α-helical cytokine that binds to a multisubunit receptor expressed on the surface of a variety of cell types. IL-2Rα, IL-2Rβ, and IL-2Rγc receptor subunits expressed on the surface of cells may aggregate to form distinct binding sites of differing affinities. IL-2Rγc was the last receptor subunit to be identified. It has since been shown to be shared by at least five other cytokine receptors. In this study, we have probed the role of IL-2Rγc in the assembly of IL-2R complexes and in ligand binding. We demonstrate that in the absence of ligand IL-2Rγc does not possess detectable affinity for IL-2Rα, IL-2Rβ, or the pseudo-high-affinity binding site composed of preformed IL-2Rα/β. We also demonstrate that IL-2Rγc possesses an IL-2-dependent affinity for IL-2Rβ and IL-2Rα/β. We performed a detailed biosensor analysis to examine the interaction of soluble IL-2Rγc with IL-2-bound IL-2Rβ and IL-2-bound IL-2Rα/β. The kinetic and equilibrium constants for sIL-2Rγc binding to these two different liganded complexes were similar, indicating that IL-2Rα does not play a role in recruitment of IL-2Rγc. We also determined that the binding of IL-2 to the isolated IL-2Rγc was very weak (approximate K_D = 0.7 mM). The experimental methodologies and principles derived from these studies can be extended to at least five other cytokines that share IL-2Rγc as a receptor subunit.

The high-affinity interleukin-2 receptor ($K_D \approx 10$ pM) is comprised of three different subunits (IL-2Rα, IL-2Rβ, and IL-2Rγc),[1] all of which interact with ligand in the cell surface complex (*1*−*3*). Although individually these subunits display weak or moderate equilibrium dissociation constants for IL-2, when they are expressed in combination, the resulting complexes exhibit greatly enhanced affinities. The IL-2Rα and IL-2Rβ subunits may associate in the absence of ligand to form the pseudo-high-affinity site (IL-2Rα/β) with a $K_D \approx 300$ pM (*4*−*6*). After this site binds IL-2, the γ-subunit (IL-2Rγc) binds to this complex to initiate signaling (*7*, *8*). In addition, in some NK cells that lack IL-2Rα, IL-2Rγc may form a complex with IL-2Rβ in the presence of ligand, resulting in the intermediate-affinity site (IL-2Rβ/γc) having a $K_D \approx 1$ nM (*9*, *10*). IL-2Rγc is also known to be a common subunit shared by the receptors for IL-4, IL-7, IL-9, IL-13, and IL-15 (*3*, *11*).

In this study, we have employed surface plasmon resonance biosensor analysis in addition to other techniques in order to elucidate the role of IL-2Rγc in the formation of high- and intermediate-affinity IL-2R receptor complexes and to demonstrate that the IL-2Rα subunit does not participate in the recruitment of IL-2Rγc.

MATERIALS AND METHODS

Protein Expression and Purification. Restriction and modifying enzymes were purchased from either Life Technologies/Gibco BRL or New England Biolabs, each supplied with its appropriate, concentrated buffers and utilized according to the manufacturer's recommendations. All chemical reagents used were of the highest research grade possible. Recombinant IL-2 was prepared as described previously (*12*). Reverse-phase HPLC was used to assess the purity of IL-2

[†] This work was supported by grants form the Veterans Administration (T.L.C.), the National Institutes of Allergy and Infectious Diseases (AI34331, T.L.C.), the National Institute of General Medical Sciences (GM35556, B.G.), and the National Science Foundation (NSF931404, T.M.L.). Support from the Norris Cotton Cancer Center (NIH CA23108) is gratefully acknowledged.

* To whom correspondence should be addressed at Dartmouth Medical School.

[‡] The University of Michigan Medical School.

[§] University of Utah.

[||] GlaxoSmithKline Pharmaceuticals.

[⊥] Los Alamos National Laboratory.

[#] University of New Hampshire.

[△] Veterans Administrations Hospital.

[▽] Dartmouth Medical School.

[1] Abbreviations: IL-2, interleukin-2; IL-2R, interleukin-2 receptor; IL-2Rα, interleukin-2 receptor α-subunit; IL-2Rβ, interleukin-2 receptor β-subunit; IL-2Rγc, interleukin-2 receptor γ-subunit; K_D, equilibrium dissociation constant; k_a, association rate constant; k_d, dissociation rate constant; $s_{20,w}$, sedimentation coefficient; RU, resonance unit.

10.1021/bi011692m CCC: $22.00
Published on Web 01/29/2002

and IL-2R subunits throughout the expression, purification, and refolding process. IL-2R subunits were expressed using the *Spodoptera frugiperda* cell line Sf9 for recombinant baculovirus production and High Five cells for protein production.

High Five cells were maintained in suspension cultures at 28 °C. Cells were cultured in baffled flasks with the shaker set at 100 rpm using EX-CELL 405 media with L-glutamine (JRH Biosciences) + antibiotic−antimycotic to 1× (Life Technologies). Cells were passaged from a density no greater than 6×10^6 cells mL^{-1} and reseeded to 1×10^6 cells mL^{-1}. High Five cells were passaged no more than 50 times. Cryopreserved aliquots were expanded in 175 cm^2 flasks using EX-CELL media supplemented with 10% FBS and 1× antibiotic−antibiotic (Life Technologies).

IL-2Rα and the S111C mutant of IL-2Rβ were expressed and purified as described previously (*6*, *13*, *14*). The purification of IL-2Rγc was carried out via a three-step purification facilitated by the presence of a hexaHis-tag sequence on the C-terminus. After filtration, the supernatant harvested from the transduction of HighFive cells with IL-2Rγc encoding baculovirus was concentrated 10-fold. The concentrate was dialyzed against buffer A (20 mM imidazole, 50 mM sodium phosphate, 500 mM NaCl, pH 8) for 12 h. The concentrated supernatant was applied to a NiNTA Superflow column (Qiagen) over 5 h. The column was washed using buffer A until a stable UV baseline was achieved at 280 nm. The bound proteins were then eluted using a linear gradient of buffer B (500 mM imidazole, 50 mM sodium phosphate, 500 mM NaCl, pH 8) using a BIOlogic FPLC system (Bio-Rad, Hercules, CA). The protein-containing fractions were collected, analyzed by rpHPLC, and pooled.

The pooled protein-containing fractions collected from metal-affinity chromatography were dialyzed into buffer C (20 mM sodium phosphate, pH 6.0) for cation-exchange chromatography using a MonoS EconoPac cartridge (Bio-Rad). Dialyzed samples were filtered prior to injection onto a MonoS column. The bound protein was eluted from the MonoS column by employing a linear gradient of buffer D (20 mM sodium phosphate, 1 M NaCl, pH 6). The protein-containing fractions were collected and analyzed by rpHPLC.

The IL-2Rγc protein-containing fractions were dialyzed into buffer E (25 mM NaH_2PO_4, 150 mM NaCl, pH 7.2). The dialysate was concentrated, loaded onto a Superose 12 SEC column (Pharmacia, Uppsala, Sweden), and separated using running buffer E on a BIOlogic FPLC system (Bio-Rad, Hercules, CA). The IL-2Rγ eluted in three fractions: a high MW irreversibly aggregated complex, a dissociable complex having an elution volume consistent with a trimer, and a lower MW fraction having an elution volume consistent with a monomer (based on previous column calibration using gel filtration standards; Sigma-Aldrich, St. Louis, MO). The latter two fractions were combined and used for subsequent experiments.

Ultracentrifugation. Ultracentrifugation analysis of the complexes was performed at the centrifugation facility at the University of New Hampshire on a Beckman XL-A analytical ultracentrifuge equipped with Rayleigh interference optics as previously described (*15*). Sedimentation velocity was conducted at 45000 rpm, and the sedimentation coefficient distributions [g(s*)] were determined from the time derivative of the concentration profile (*15*). The complexes were prepared by taking samples of the proteins prepurified by gel filtration as described above and mixing IL-2 with equimolar aliquots of the appropriate receptor subunits in buffer E. The samples were then concentrated to greater than 5 mg/mL for analysis. The complex of IL-2•IL-2Rβ•IL-2Rγc displayed sufficient stability to allow isolation by gel filtration after mixing and concentration of the individual components (*16*). The fraction corresponding to the complex was isolated by gel filtration as described above and concentrated to greater than 5 mg/mL for analysis (rechromatography indicated no dissociation).

BIACORE Biosensor Analysis. All analyses were carried out on a BIACORE 2000 at 25 °C. Research grade CM5 sensor chips, *N*-hydroxysuccinimide (NHS), *N*-ethyl-*N*′-(3-diethylaminopropyl)carbodiimide (EDC), and ethanolamine hydrochloride were purchased from the manufacturer (BIACORE Inc., Piscataway, NJ). Ethylenediamine and L-cysteine were purchased from Sigma-Aldrich (St. Louis, MO). HCl (10 mM) was prepared from concentrated HCl (Fisher Scientific, Pittsburgh, PA). Sulfo-MBS (*m*-maleimidobenzoyl-*N*-hydroxysulfosuccinimide ester) was purchased from Pierce Chemicals (Pierce, Rockford, IL). All buffers were filtered and degassed daily.

For amine coupling, carboxymethylated dextran surfaces on CM5 chips were activated using the standard NHS/EDC procedure. Proteins were diluted to no less than 20 nM in 10 mM sodium acetate, pH 5. The diluted proteins were injected over the activated surface until the desired surface densities were achieved. Activated, coupled surfaces were then quenched of reactive sites with 1 M ethanolamine, pH 8, for 7 min.

For thiol-mediated coupling of IL-2Rα and IL-2Rβ (*6*), carboxymethylated dextran surfaces on CM5 chips were activated using NHS/EDC for 7 min followed by sequential 7 min injections of 1 M ethylenediamine, pH 8.5, and 1 M ethanolamine, pH 8. The surfaces were then treated for 7 min with *m*-maleimidobenzoyl-*N*-hydroxysulfosuccinimide ester (Sulfo-MBS;, Pierce, Rockford, IL) reconstituted at 20 mg mL^{-1} in 25 mM $NaHCO_3$, pH 8.5. Proteins to be thiol coupled were diluted to no less than 20 nM in 10 mM sodium acetate, pH 5, and injected over the activated surface until the desired surface densities were achieved. The thiol-reactive surface was quenched with a 7 min exposure using L-cysteine, 20 mg mL^{-1} in 1 mM HCl, prepared immediately prior to injection.

For the preparation of IL-2Rγc surfaces, a surface of 3470 RU of an anti-tetraHis monoclonal antibody (Qiagen) was prepared via standard amine coupling as described above. Then, prior to each IL-2 injection, 3000 RU of sIL-2Rγc was captured via its C-terminal His tag. After IL-2 injection, the surface was stripped of IL-2 and IL-2Rγc by a 5 s injection of 10 mM HCl.

All data were collected at 10 Hz using at least three to four replicate injections for each determination. Flow rates during experiments were maintained at 100 μL min^{-1}. Regeneration of active surfaces (when necessary) was carried out by 9 s injection of 10 mM HCl. For the study of the binding of the soluble IL-2Rγc subunit to IL-2-occupied IL-2Rβ surfaces, sIL-2Rγc and IL-2 were injected simultaneously. The binding of sIL-2Rγc to IL-2-occupied IL-2Rα/β surfaces was monitored by first injecting IL-2 and waiting

for bound ligand to dissociate from all occupied IL-2Rα and IL-2Rβ sites, leaving only occupied IL-2Rα/β sites prior to injection of sIL-2Rγc. Reference surfaces consisted of bovine serum albumin (BSA) of comparable surface densities. The reference surface for measuring IL-2 binding (single injections) to IL-2Rγc captured by an anti-tetraHis MAb consisted of an equivalent surface density of MAb without IL-2Rγc present. All final data sets were double referenced (*17*) and edited using Microsoft Excel. Edited sensorgram data sets were analyzed using CLAMP (*18*, *19*).

Analysis of Biosenor Data. The kinetic biosensor data were globally fit to the appropriate binding models using CLAMP (*19*). The raw experimental data were corrected for instrumental and bulk solvent artifacts by double referencing using both activated and blocked surfaces as controls (*17*). The influence of mass transport on IL-2 binding was accounted for by including a mass transport variable using a two-compartment model (*20*). Thus, for the single site binding of IL-2 to individual homogeneous receptor surfaces, data were fit to model 1 (eq 1), where IL-2_0 represents the concentration of IL-2 in the bulk flow and k_m represents the transport rate constant to and from the unstirred layer (*20*).

$$(1)\ \text{IL-}2_0 \underset{k_m}{\overset{k_m}{\rightleftharpoons}} \text{IL-2} \qquad (1)$$

$$(2)\ \text{IL-2} + \text{IL-2R}_x \underset{k_d}{\overset{k_a}{\rightleftharpoons}} \text{IL-2·IL-2R}_x$$

To describe the binding of IL-2 to the biosensor surface consisting of both IL-2Rα and IL-2Rβ subunits forming the pseudo-high-affinity IL-2R site, three types of binding events must be considered: (1) the binding of IL-2 to IL-2α alone, (2) the binding of IL-2 to IL-2Rβ alone, and (3) the binding of IL-2 to the preformed pseudo-high-affinity site, IL-2Rα/β (*6*). Thus the complete model 2 (eq 2) employed for fitting data obtained on this surface is

$$(1)\ \text{IL-}2_0 \underset{k_m}{\overset{k_m}{\rightleftharpoons}} \text{IL-2} \qquad (2)$$

$$(2)\ \text{IL-2} + \text{IL-2R}\alpha \underset{k_d}{\overset{k_a}{\rightleftharpoons}} \text{IL-2·IL-2R}\alpha$$

$$(3)\ \text{IL-2} + \text{IL-2R}\beta \underset{k_d}{\overset{k_a}{\rightleftharpoons}} \text{IL-2·IL-2R}\beta$$

$$(4)\ \text{IL-2} + \text{IL-2R}\alpha\beta \underset{k_d}{\overset{k_a}{\rightleftharpoons}} \text{IL-2·IL-2R}\alpha\beta$$

The association and dissociation rate constants for the binding of IL-2 to the individual IL-2Rα and IL-2Rβ subunits and the mass transport rate constant determined using model 1 were fixed to those values in data analyses using model 2. The kinetic rate constants for step 4 and the maximum surface densities of all of the receptor species were the floating parameters in this model.

Since preliminary experiments indicated that surfaces prepared by covalent attachment of IL-2Rγ were not stable to the repeated regeneration conditions required for the acquisition of high-quality kinetic data, we employed a soluble version of the γ-subunit (sIL-2Rγc). This protein was injected either simultaneously with IL-2 for binding to homogeneous IL-2Rα or IL-2Rβ surfaces or co-injected alone on mixed IL-2Rα/β surfaces pretreated with IL-2. In the former experiments, the model 3 (eq 3) was employed for data analysis:

Table 1: Sedimentation Velocity Results

receptor complex	$s_{20,w}$ (S)
IL-2Rβ·sIL-2Rγc·IL-2	4.8
IL-2Rβ·IL-2	3.2
IL-2Rβ	2.1

$$(1)\ \text{IL-}2_0 \underset{k_m}{\overset{k_m}{\rightleftharpoons}} \text{IL-2} \qquad (3)$$

$$(2)\ \text{IL-2} + \text{IL-2R}_x \underset{k_d}{\overset{k_a}{\rightleftharpoons}} \text{IL-2·IL-2R}_x$$

$$(3)\ \text{IL-2·IL-2R}_x + \text{sIL-2R}\gamma\text{c} \underset{k_d}{\overset{k_a}{\rightleftharpoons}} \text{IL-2·IL-2R}_x\text{·sIL-2R}\gamma\text{c}$$

As in model 2, the kinetic rate constants for IL-2 binding to the individual surface subunits and the mass-transport rate constants were fixed to the previously determined values. Analysis of preliminary experiments indicated that binding of sIL-2Rγc was not mass-transport limited so no corresponding variable was added to the model. An additional term was used to correct for the differences in refractive index increment between IL-2 and sIL-2Rγc (*21*).

In the case of the binding of sIL-2Rγc to a mixed IL-2Rα/β surface pretreated with IL-2, the experiment was designed so that only pseudo-high-affinity IL-2Rα/β sites were occupied by IL-2 at the time of sIL-2Rγc injection (see Results); thus model 3 was employed for data analysis where IL-$2R_x$ is IL-2Rα/β.

Competitive Radioligand Binding. Competitive binding assays were performed as described (*21*) using 0.5 nM ^{125}I-IL-2 on the MT-1 human T cell leukemia cell line (*9*). Briefly, cells were cultured in RPMI + 10% FBS and 50 μg mL^{-1} gentamycin and were washed three times with buffer E prior to using them in the assays at 4×10^6 cells per binding tube. Twofold serial dilutions of mixtures (starting at 10 μM) of soluble IL-2Rβ and IL-2Rγc at 1:1, 1:9, and 9:1 molar ratios were employed as competitors. Twofold serial dilutions of IL-2 (starting at 3 μM) served as a positive control and to establish total binding and nonspecific binding. Analysis of the binding data from these experiments was attempted using procedures similar to those previously described (*22*).

RESULTS

Ultracentrifugation Analysis of IL-2R Complexes. Mixing of IL-2 with the soluble forms of IL-2Rβ and IL-2Rγc led to the formation of a complex that was stable enough to be isolated by gel filtration chromatography (*16*). In our hands, both monomeric sIL-Rγc and trimeric sIL-2Rγc could be completely converted to the IL-2·IL-2Rβ·IL-2Rγc complex by addition of excess IL-2 and sIL-2Rβ, while only the high molecular weight sIL-2Rγc aggregate was nonreactive (not shown). Since this complex was stable upon size exclusion rechromatography, we carried out sedimentation velocity experiments to obtain an estimate of its molecular size. The results are shown in Table 1. The complex of IL-2·IL-2Rβ·IL-2Rγc migrated at $s_{20,w} = 4.8$ S, consistent with trimeric stoichiometry. While we did not examine the behavior of

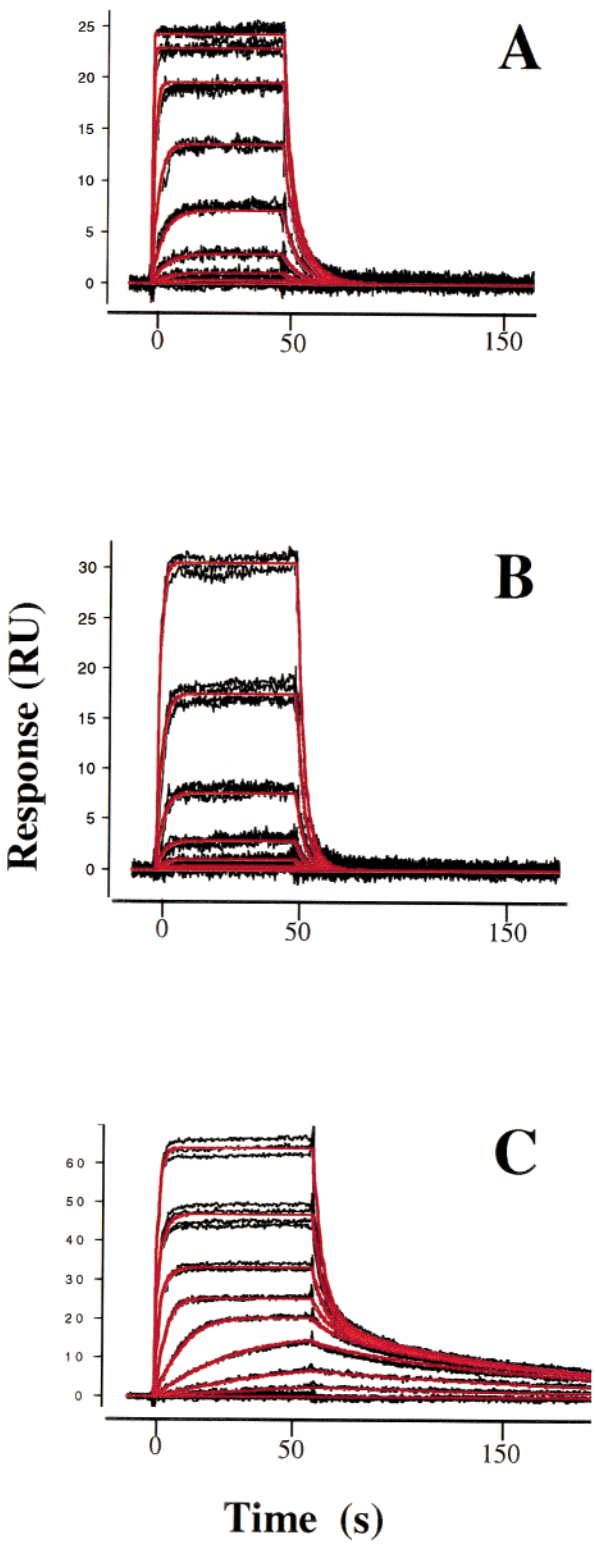

FIGURE 1: Kinetic response data for IL-2 binding to biosensor surfaces containing IL-2Rα and IL-2Rβ subunits. Experimental data (black) represent quadruplicate injections of each IL-2 concentration (see Materials and Methods) over surfaces containing (A) 150 RU of IL-2Rα, (B) 220 RU of IL-2Rβ, and (C) 470 RU of IL-2Rβ plus 163 RU of IL-2Rα at a flow rate of 100 μL/min. Global fits of these data according to the models described in Materials and Methods are depicted in red, and the resulting kinetic constants are listed in Table 2.

IL-2Rγc because of its known tendency to form multiple aggregates, IL-Rβ alone migrated at $s_{20,w} = 2.11$ S, and upon addition of IL-2 the sedimentation coefficient increased to 3.24 S. This indicates that, unlike IL-2Rγc, the soluble form of IL-Rβ is monomeric and will interact with IL-2 at concentrations consistent with its apparent K_D of >400 nM (*6*, *14*). Therefore, in solution at the concentrations studied these components interact with simple stoichiometry to form a stable IL-2·IL-2Rβ·IL-2Rγc trimeric complex.

Table 2: Binding Parameters Determined by Biosensor Analysis

analyte/surface	k_a (M^{-1} s^{-1})	k_d (s^{-1})	K_D (k_d/k_a)
IL-2/IL-2Rα	1.06(2)[a] × 10^7	0.298(4)	28.1(6) nM
IL-2/IL-2Rβ	5.84(4) × 10^5	0.312(2)	534(5) nM
IL-2/IL-2Rα/β	1.69(2) × 10^7	0.018(1)	1.07(6) nM
IL-2/IL-2Rγc	ND[b]	ND[b]	0.7 mM
sIL-2Rγc/IL-2·IL-2Rβ	3.44(9) × 10^4	5.09(2) × 10^{-3}	150(30) nM
sIL-2Rγc/IL-2·IL-2Rα/β	1.78(2) × 10^4	3.22(7) × 10^{-3}	180(50) nM

[a] Values in parentheses represent the standard deviation in the final significant digit. [b] Not determined.

Biosensor Analysis of Ligand Binding to IL-2Rα and IL-2Rβ Surfaces. To examine the role of IL-2Rγc in IL-2 binding to receptor complexes on biosensors, we extended studies that we have previously described (*6*). Values for the kinetic parameters reported in those studies were also needed to fit the more complex models that include IL-2Rγc in this study. Since these experiments were carried out on a different instrument platform with freshly prepared reagents, we repeated the earlier analyses of the interaction of IL-2 with IL-2Rα, IL-2Rβ, and mixed surfaces to corroborate the earlier results and provide contemporary values of the kinetic parameters needed for analysis of binding models that include IL-2Rγc.

Biosensor Analysis of IL-2 Binding to Homogeneous IL-2Rα and IL-2Rβ Surfaces. To test the fidelity of the IL-2Rα/IL-2 interaction, IL-2 was injected over a thiol-coupled IL-2Rα biosensor surface as described previously (*6*). Quadruplicate IL-2 samples were injected at concentrations of 900, 300, 100, 33, 11, 3.7, 1.2, and 0.41 nM (Figure 1A). The values for the kinetic binding constants (k_d and k_a) are shown in Table 2 and were determined by globally fitting the data shown in Figure 2A to a single site binding model 1 limited by mass transport as described (*6*). The mass transport rate (k_m) obtained for diffusion of IL-2 to and from the sensor surface was 2.17 × 10^8 RU/(m s). The K_D as determined from the ratio of these constants was 28.1 nM (consistent with the value of 31 nM previously determined; *6*).

Similarly, quadruplicate injections of IL-2 samples at 900, 300, 100, 33, 11, 3.7, 1.2, and 0.41 nM over a thiol-coupled IL-2Rβ biosensor surface (*6*) produced the data shown in Figure 1B. Global fitting of these data to model 1 yielded the kinetic rate constants listed in Table 2. Again, the K_D determined from the ratio these kinetic rate constants (k_d/k_a) for IL-2 binding the IL-2Rβ compared very favorably with our previous study (534 vs 500 nM).

Biosensor Analysis of IL-2 Binding to Mixed IL-2Rα /IL-2Rβ Surfaces. To simulate the binding of IL-2 to the pseudo-high-affinity IL-2Rα/β receptor, a heterogeneous surface consisting of both IL-2Rα and IL-2Rβ was prepared as described (*6*). Quadruplicate IL-2 samples at concentrations of 900, 300, 100, 33, 11, 3.7, 1.2, and 0.41 nM were injected over a thiol-coupled biosensor surface consisting of a 3-fold

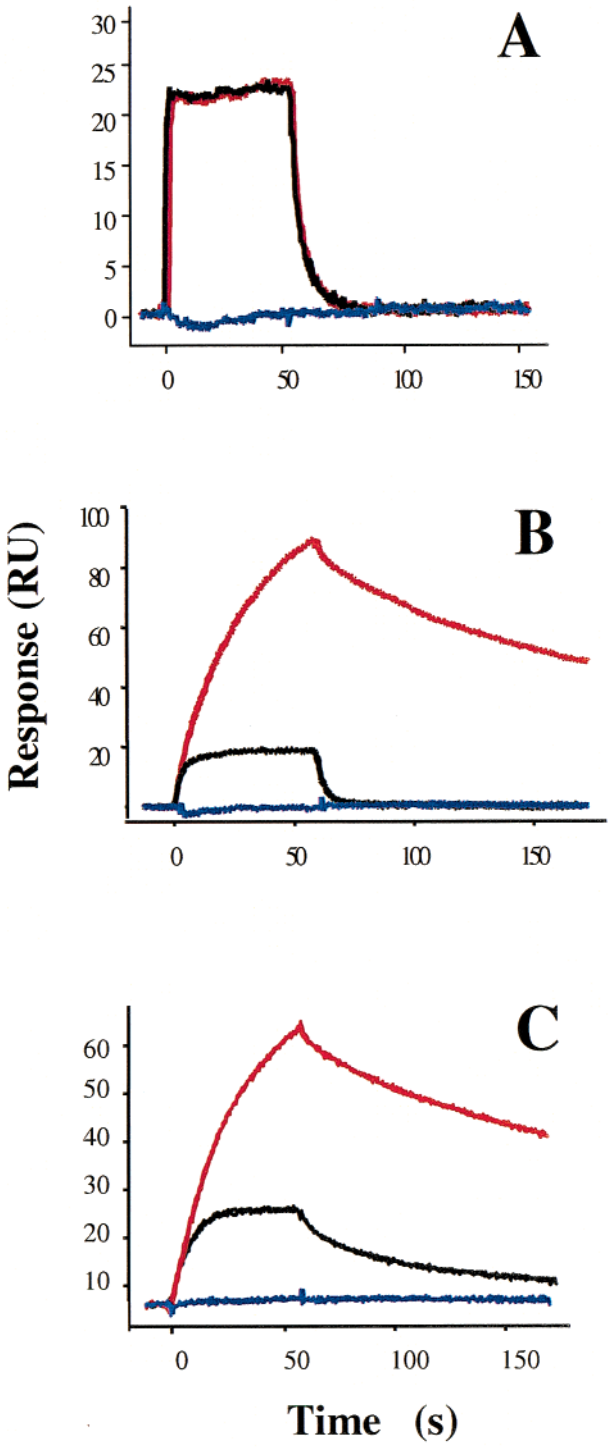

FIGURE 2: Binding of IL-2 and sIL-2Rγc to biosensor surfaces prepared from (A) 150 RU of IL-2Rα, (B) 220 RU of IL-2Rβ, and (C) 470 RU of IL-2Rα plus 163 RU of IL-2Rβ. Black sensorgrams represent duplicate injections of IL-2 alone [300 nM in (A) and (B), 11 nM in (C)]; blue sensorgrams represent duplicate injections of sIL-2Rγc alone (3 μM); red sensorgrams represent duplicate injections of a mixture of IL-2 [300 nM in (A) and (B), 11 nM in (C)] and sIL-2Rγc (3 μM).

molar excess of IL-2Rβ to IL-2Rα (Figure 1C). Global fitting of the data collected from this mixed surface to model 2 provided the kinetic constants listed in Table 2. Although the k_a obtained for the mixed surface was less than 2-fold faster than for the IL-2Rα surface (Table 2), model 2 provided the best fit to the data when compared to fits by other models (not shown) including the "affinity conversion"

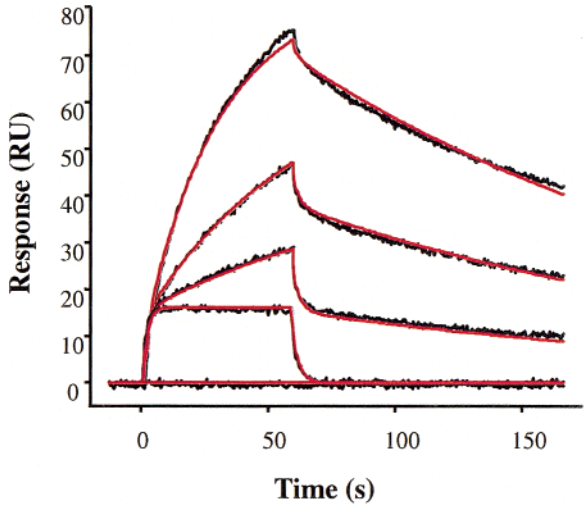

FIGURE 3: Kinetic response data for a mixture of IL-2 and sIL-2Rγc binding to a biosensor surface containing IL-2Rβ (220 RU). Experimental data (black) represent the average of quadruplicate injections of mixtures of a constant concentration of IL-2 (300 nM) and varying concentrations of sIL-2Rγc (3.0 μM, 1.0 μM, 0.33 μM, and 0) at a flow rate of 100 μL/min. Global fits of these data according to model 3 described in Materials and Methods are depicted in red, and the resulting kinetic constants are listed in Table 2.

model (*6*). As in our previous study, a pseudo-high-affinity site was detected possessing a K_D (1.07 nM, determined from the ratio of the kinetic rate constants) significantly lower than the K_Ds for either of the individual subunits. The increase in affinity at this preformed IL-2Rα/β site is primarily attributable to a slower dissociation rate constant than was observed for either of the single subunit surfaces.

Having established the reproducibility of the biosensor assay, the analysis was expanded to study the role of IL-2Rγc in the formation of the intermediate- and high-affinity receptor complexes.

Biosensor Analysis of the Binding of sIL-2Rγc to IL-2 Occupied Receptor Surfaces. IL-2Rγc is not productively associated with either the β-subunit or the pseudo-high-affinity complex prior to IL-2 binding; rather it binds in a ligand-dependent fashion to form the intermediate- and high-affinity signaling complexes (*8*, *23*, *24*). Since direct immobilization of IL-2Rγ yielded unstable surfaces, we employed a soluble version comprised of the receptor extracellular domain to study the ligand-dependent recruitment of this subunit.

First, a biosensor surface consisting of 150 RU of IL-2Rα was prepared via thiol-mediated coupling. At 3 μM, sIL-2Rγc did not possess a measurable affinity for the IL-2Rα surface, either unoccupied or occupied by IL-2 (300 nM) (Figure 2A).

Likewise, sIL-2Rγc (3 μM) did not bind to a biosensor surface consisting of 220 RU of IL-2Rβ alone (Figure 2B). However, when sIL-2Rγc was injected as a mixture with 300 nM IL-2, a significant increase in RU was observed compared to the binding of 300 nM IL-2 alone, and the complex was considerably more stable, requiring an acid wash to regenerate the surface. This clearly demonstrated that the interaction of sIL-2Rγc and IL-2Rβ was IL-2 dependent. Similar results were observed when sIL-2Rγc was injected in the presence and absence of IL-2 over a mixed

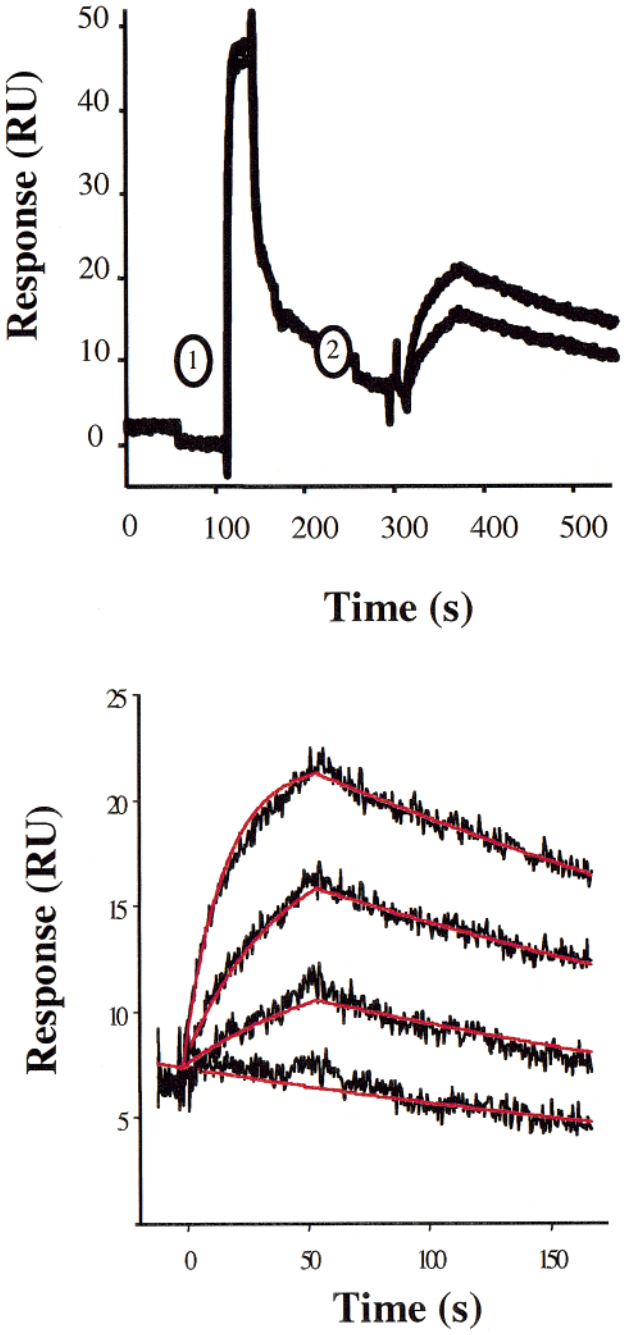

FIGURE 4: Top: Sequential injection protocol for the analysis of binding of sIL-2Rγc to an IL-2 occupied IL-2Rα/β surface. (1) represents injection of 300 nM IL-2 and (2) represents subsequent injections of sIL-2Rγc. Bottom: Kinetic response data for sIL-2Rγc binding to an IL-2 occupied IL-2Rα/β surface (470 RU of IL-2Rα plus 163 RU of IL-2Rβ). Experimental data (black) represent the average of quadruplicate injections of varying concentrations of sIL-2Rγc (3.0 μM, 1.0 μM, 0.33 μM, and 0) after a prior injection of 300 nM IL-2 according to the protocol above, at a flow rate of 100 μL/min. Global fits of these data according to model 3 described in Materials and Methods are depicted in red, and the resulting kinetic constants are listed in Table 2.

biosensor surface of 163 RU of IL-2Rα and 470 RU of IL-2Rβ to form the IL-2Rα/β pseudo-high-affinity site. Only in the presence of IL-2 (300 μM) did sIL-2Rγc bind to the surface, as indicated by the significant increase in RU when compared to the injection of IL-2 alone (Figure 2C).

The binding kinetics of sIL-2Rγc to IL-2Rβ and IL-2Rα/β occupied by IL-2 appeared qualitatively identical (Figure 2B,C). To determine if the binding of sIL-2Rγc to these different surfaces displayed similar kinetics, we carried out experiments designed to determine precise values for the kinetic binding constants.

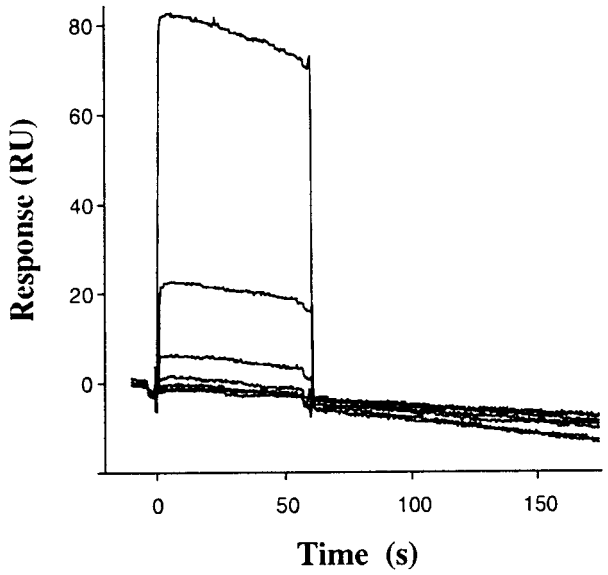

FIGURE 5: Binding of IL-2 to a biosensor surface prepared from 3000 RU of IL-2Rγc immobilized via a His tag to an anti-4×His monoclonal antibody surface. Sensorgrams represent injections of varying concentrations of IL-2 (60, 20, 6.6, 2.2, and 0.74 μM) after subtraction of nonspecific responses obtained from the same injections passing over a second surface of 3500 RU of anti-4×His monoclonal antibody alone. The K_D obtained from these data is listed in Table 2.

To determine association and dissociation rate constants for sIL-2Rγc binding to IL-2-occupied IL-2Rβ, IL-2 and sIL-2Rγc were co-injected over a 220 RU IL-2Rβ surface. In this series, the IL-2 concentration was fixed at 300 nM, and the concentration of sIL-2Rγc was varied (3.0 μM, 1.0 μM, 0.33 μM, and 0). The data obtained from the average of quadruplicate injections at each concentration (Figure 3) were fit globally to model 3. The corresponding values for the association and dissociation rate constants for sIL-2Rγc are displayed in Table 2. These constants are significantly slower than for the binding of IL-2 to IL-2Rβ, confirming that, during simultaneous injection, sIL-2Rγc binds only to IL-2-occupied sites. The K_D for sIL-2Rγc binding to IL-2·IL-2Rβ as determined from the ratio of the kinetic constants was 150 ± 30 nM.

To compare these results with kinetic constants for sIL-2Rγc binding to IL-2-occupied sites on a pseudo-high-affinity IL-2Rα/β surface, a heterogeneous surface was prepared consisting of 163 RU of IL-2Rα and 470 RU of IL-2Rβ. To ensure that all of the binding observed was interactions between sIL-2Rγc and occupied IL-2Rα/β sites and not occupied individual receptor sites, a double injection protocol was developed that exploited the slower dissociation rate of IL-2 from IL-2Rα/β. First, IL-2 (300 nM) was injected by itself over the heterogeneous surface. Then at the end of the injection, dissociation was allowed to proceed for 180 s. Preliminary experiments demonstrated that this period was sufficient to allow any IL-2 bound to individual α- or β-subunits to completely dissociate, leaving only IL-2Rα/β sites occupied (Figure 4, top). Finally, a second injection containing sIL-2Rγc (3.0, 1, and 0.33 μM) was per-

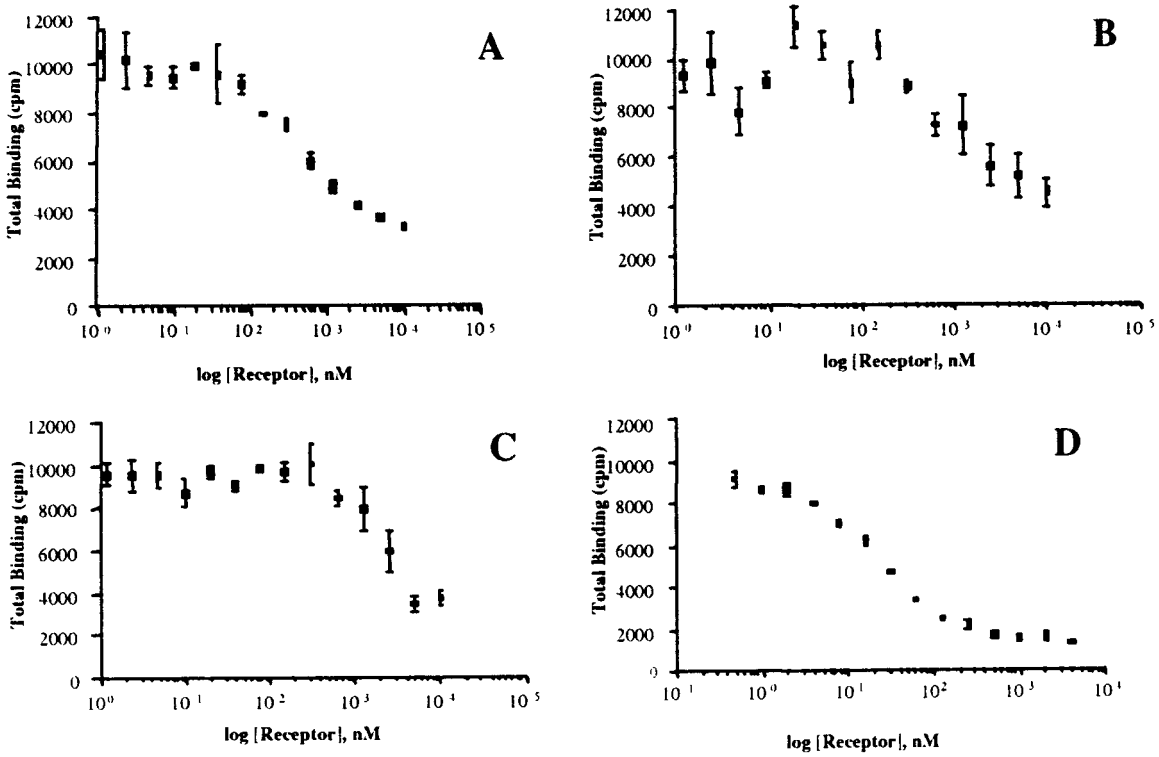

FIGURE 6: Competitive displacement of ^{125}I-IL-2 on MT-1 cells by (A) a 1:1 mixture of sIL-2Rβ and sIL-2Rγc, (B) a 9:1 mixture of sIL-2Rβ and sIL-2Rγc, (C) a 1:9 mixture of sIL-2Rβ and sIL-2Rγc, and (D) an unlabeled IL-2 control. The data points represent the mean of triplicate determinations (with standard error indicated) of 2-fold serial dilutions beginning with a total concentration of soluble receptor of 10 μM (A−C) and 4 μM IL-2 (D).

formed. The data obtained from the average of quadruplicate injections at each concentration (Figure 4, bottom) were fit globally to model 3. In this experiment, the initial concentration of IL-2 at the time of injection of sIL-2Rγc was 0 (no IL-2 was present in the injected sample), and the rate constants for IL-2 binding to IL-2Rα/β were fixed to the values previously determined (Table 2). The values obtained for the association and dissociation rate constants for the binding of sIL-2Rγc to occupied IL-2Rα/β sites are displayed in Table 2. The K_D for this interaction determined from the ratio of the kinetic constants was 180 $\pm$ 50 nM.

Biosensor Analysis of IL-2 Binding to IL-2Rγc. To confirm that the interaction of IL-2 with sIL-2Rγc was sufficiently weak to be neglected in the above studies, we designed experiments to attempt to detect direct binding of IL-2 to sIL-2Rγc. Biosensor surfaces prepared by covalent attachment of IL-2Rγc directly to the dextran layer were found to be too sensitive to regeneration methods to allow the collection of high-quality replicate data sets required for kinetic analysis. This was not unexpected since even cell surface IL-2Rγc is known to be unstable to denaturants (*25*). Therefore, the binding of IL-2 to IL-2Rγc was studied by capturing 3000 RU of IL-2Rγc via its C-terminal His tag on 3470 RU of an anti-4×His monoclonal antibody surface. A control surface consisting of 3500 RU of the same antibody was employed to correct for nonspecific binding. IL-2 was injected over each surface at concentrations of 60, 20, 6.6, 2.2, and 0.74 μM (Figure 5). The data set comprised of single determinations of steady-state binding levels at each concentration after correction for nonspecific binding was fit to a simple single site binding isotherm. This limited data set provided an approximate K_D value of 0.70 mM for the binding of IL-2 to IL-2Rγc. This value is consistent with earlier reports that this interaction is extremely weak (*26*, *27*) and therefore can be ignored in our kinetic analysis.

Competitive Radioligand Binding. To corroborate the equilibrium dissociation constant obtained by biosenor analysis for the binding of sIL-2Rγc to occupied IL-2Rβ, we carried out competitive binding experiments using MT-1 cells expressing only the IL-Rα receptor (*9*). Ultracentrifugation analysis demonstrated that a mixture of sIL-2Rγc and sIL-2Rβ could form a stable complex with IL-2 in solution and therefore should compete for the binding of IL-2 to cell surface receptors. To provide a more extensive data set, three different ratios of sIL-2Rγc to sIL-2Rβ were employed (9:1, 1:1, 1:9) and were serially diluted 2-fold beginning with a total receptor concentration of 10 μM. The results of these experiments are shown in Figure 6. These assays demonstrate that each mixture was capable of competing for the binding of ^{125}I-IL-2 to cell surface IL-2Rα; however, none of them could compete to the background level of nonspecific binding observed when unlabeled IL-2 was employed as a control. Similar results were observed in our previous study of IL-2R$\beta\gamma$ coiled-coil complexes (*22*). In those experiments, the data were fit to models that allowed IL-2 bound to soluble receptor complexes to bind further to cell surface receptors. Interaction of IL-2 with sIL-2Rβ or with sIL-2Rβ and sIL-2Rγc does not necessarily preclude further interaction with cell surface IL-2Rα. That is, even though bound to a soluble receptor or receptor complex in solution, the IL-2 in these complexes may still be capable of interacting with cell surface receptors such that complete competition for labeled IL-2 does not occur. In the current study where sIL-2Rβ and sIL-2Rγc are not preassociated in solution, models allowing for all of the potential equilibria that might occur contained too many variables to enable precise fitting of the data in

Figure 6. Therefore, only a qualitative assessment of the competitive efficiency of mixtures of sIL-2Rβ and sIL-2Rγc could be made. The best results were achieved with a 1:1 mixture (Figure 6A) having an IC_{50} for competable cpm of less than 500 nM. This value appears to be consistent with the K_D of 150 nM obtained by biosensor analysis for the association of sIL-2Rγc to IL-2·sIL-2Rβ.

DISCUSSION

The goal of this study was to characterize the role of IL-2Rγc in the formation of the high- and intermediate-affinity IL-2 receptor complexes. Since these two receptors appear on cell types with varying functions, any differences in the role of IL-2Rγc in ligand binding could provide an avenue for the design of selective therapeutics. Early studies of the ligand binding properties of IL-2Rγc suggested that interaction with IL-2 in the absence of other receptor subunits was very weak at best (*26*, *27*). Furthermore, signaling processes requiring the participation of IL-2Rγc were entirely dependent upon IL-2 mediated cross-linking of this subunit with IL-2Rβ (*7*, *8*). Our results are consistent with these conclusions. The use of soluble forms of the IL-2R subunits comprised only of their extracellular domains facilitated a more quantitative approach to the analysis of ligand binding. When expressed in insect cells, sIL-2Rγc was isolated as a mixture of monomeric and aggregated forms (a trimeric form and a higher molecular weight aggregate). When mixed in solution with IL-2 and sIL-2Rβ, both the monomeric and trimeric forms of sIL-2Rγc were capable of generating a single complex stable enough to be isolated by gel filtration chromatography. Sedimentation velocity analysis of this complex yielded a sedimentation coefficient consistent with heterotrimeric stoichiometry. Therefore, it was clear that sufficient recognition elements exist in the extracellular domains of IL-2Rβ and IL-2Rγc to allow stable ligand-mediated cross-linking.

In light of our earlier studies (*6*, *28*, *29*), these results suggested that biosensor analysis of the ligand binding properties of IL-2Rγc could provide a more quantitative view of the role of this subunit. This technology allows the selective preparation of sensor surfaces of individual as well as mixed receptor subunits; however, initial attempts at direct covalent attachment of sIL-2Rγc to the biosensor matrix proved unsatisfactory due to instability of the protein during surface regeneration. We have previously encountered sensitivity of IL-2Rγc to denaturants both as a cell surface protein (*25*) and as a soluble form during elution from immunoaffinity columns or in coiled-coil complexes (*22*). Therefore, we pursued an alternate strategy of injecting sIL-2Rγc as a coanalyte with IL-2 over surfaces bearing the other IL-2 receptor subunits. In doing so, this amounted to an extension of our earlier study of IL-2 binding to α-, β-, and mixed subunit surfaces (*6*). Since this approach required preparation of new surfaces using fresh protein samples, we repeated those earlier experiments to ensure consistency. The results shown in Figure 1 and the values obtained for the kinetic binding constants listed in Table 2 compared very favorably with our earlier results (*6*).

We then carried out experiments designed to yield the kinetic binding constants of sIL-2Rγc to IL-2-occupied IL-2Rβ and IL-2Rα/β in order to simulate the ligand-dependent recruitment of IL-2Rγc to the cell surface intermediate- and high-affinity complexes. Preliminary experiments demonstrated that sIL-2Rγc bound only to IL-2-occupied IL-2Rβ and IL-2Rα/β biosensor surfaces. sIL-2Rγc exhibited no binding to unoccupied surfaces nor to IL-2Rα surfaces (occupied or unoccupied) under the conditions tested (Figure 2B,C). These results were consistent with previous reports of the role of IL-2Rγc in ligand binding and signaling in cells (*3*, *7*, *8*, *11*). In addition, the kinetics of binding of sIL-2Rγc to IL-2-occupied receptor surfaces appeared to be much slower than for IL-2 binding to the unoccupied sites. This observation facilitated both the design and analysis of the subsequent kinetic experiments.

To determine the kinetic binding constants of sIL-2Rγc to occupied IL-2Rβ, we prepared a biosensor surface via oriented thiol coupling of a C111S IL-2Rβ analogue (*6*). Mixtures of sIL-2Rγc and IL-2 were then injected in quadruplicate over the surface (Figure 3). The concentration of IL-2 was held constant at 300 nM, sufficient to provide about 18 RU of IL-2-occupied sites. The concentration of sIL-2Rγc was varied from 3 μM to 0. It is clear from the sensorgrams in Figure 3 that the initial binding of IL-2 to IL-2Rβ is very rapid and that the association of sIL-2Rγc to these occupied sites is represented by a slower second phase. Global fitting of these data to model 3 yielded the desired association and dissociation rate constants for the binding of sIL-2Rγ to occupied IL-2Rβ (Table 2). It is interesting that the value obtained for the dissociation rate constant ($k_d = 5.09 \times 10^{-3}$ s^{-1}) is only about 10-fold faster than values reported previously for the dissociation rate constant of IL-2 from the cell surface intermediate-affinity receptor (*4*, *9*). Given the differences in methodology employed in these studies and the fact that, in this report, IL-2Rγc was a soluble rather than cell surface protein, the correspondence in these values suggests similar mechanisms.

To simulate binding of sIL-2Rγc into the high-affinity complex, a sequential injection protocol was employed over a mixed IL-2Rα and IL-2Rβ surface. In earlier studies, we have demonstrated that on the cell surface IL-2Rα and IL-2Rβ preassociate to form the pseudo-high-affinity site (*4*) and that this can be mimicked on the surface of a biosensor (*6*). For this purpose, a mixed sensor surface was prepared with an excess of IL-2Rβ in order to maximize the formation of preassociated IL-2Rα/β sites. Upon injection of IL-2 over this surface, binding may occur not only to IL-2Rα/β but also to excess IL-2Rβ and IL-2Rα sites (as indicated in model 2). Fortunately, the dissociation rate of IL-2 bound to IL-2Rα/β is considerably slower than the rates from either of the individual receptor sites. Therefore, it was possible to inject IL-2 over the mixed surface and allow enough time for complete dissociation from any occupied IL-2Rβ and IL-2Rα sites while still maintaining a sufficient number of occupied IL-2Rα/β sites to observe binding of sIL-2Rγc from a second injection (Figure 4A). Using this double injection protocol, we analyzed the binding of varying concentrations of sIL-2Rγ to about 10 RU of IL-2-occupied IL-2Rα/β sites (Figure 4B). Global fitting of the average of quadruplicate injections to model 3 provided the kinetic binding constants listed in Table 2. Neither the rate constants nor the corresponding K_D value (180 ± 50 nM) was significantly different from those obtained for the interaction of sIL-2Rγ with occupied IL-2Rβ. This finding suggests that,

in solution, there is little difference in these interactions and that the IL-2Rα subunit does not play a role in the binding of IL-2Rγc. Although missing from this approach is the orientating influence of the cell membrane on the transmembrane segment of IL-2Rγc which may aid in holding the extracellular domain in register with the other subunits, it is likely that the mechanism of cell surface recruitment is similar. Supporting this conclusion are the results of previous studies that indicate that the dissociation rate constants of IL-2 from the intermediate- and high-affinity sites are equivalent (*4*, *9*, *30*). It is possible that the IL-2Rα subunit dissociates from or remains only loosely associated with the high-affinity complex after recruitment of IL-2Rγc. After ligand-dependent internalization, the α-subunit is trafficked differently than the other IL-2R subunits (*31*).

In the biosensor analysis of sIL-2Rγc binding, it was assumed that there was little direct interaction of the protein with IL-2 in solution at the concentrations employed. To directly test this assumption, we anchored IL-2Rγc to a biosensor surface by first covalently linking an anti-His tag MAb and then capturing sIL-2Rγc via the same His tag used for purification. In this manner we were able to prepare a surface with a density of 3000 RU of sIL-2Rγc. IL-2 was injected at varying concentrations (Figure 5), and a limited data set was obtained that allowed a K_D to be estimated. The value of 0.70 mM for the equilibrium dissociation constant of the binding of IL-2 to IL-2Rγc, although approximate, is the first report of this constant and confirms the weakness of the interaction.

Attempts to use competitive radiolabeled binding methods to determine an equilibrium dissociation constant for the interaction of IL-2 with sIL-2Rβ and sIL-2Rγc met with limited success. Although competition with binding of IL-2 to cell surface α-receptors could be observed (Figure 6A), it was not complete. Reduction of binding to nonspecific background levels could not be achieved. This was likely due to the ability of the ^{125}I-IL-2·sIL-2Rβ·sIL-2Rγc complex to further interact with cell surface α-receptors at high concentrations. We have previously observed a similar phenomenon in our study of the IL-2R coiled-coil complexes (*22*). In that study we were able to successfully fit the binding data to a model that included additional binding parameters. In this case, the data could not be satisfactorily fit since models describing all of the potential solution and cell surface interactions contained too many variables, even when the ratios of IL-2Rβ to sIL-2Rγ were varied. Nevertheless, the competitive binding data were qualitatively consistent with the biosensor results. Significant competition was observed at receptor concentrations less than 1 μM (Figure 6).

In conclusion, we have provided a more quantitative view of the role of IL-2Rγc in both the intermediate- and high-affinity receptor complexes. As in earlier studies, the use of biosensor analysis proved extremely valuable and allowed examination of the binding of IL-2Rγc to ligand occupied sites. Kinetic and equilibrium binding constants were determined. The similarity of the values for these parameters for both sites suggests that the mechanism of binding of IL-2Rγc is the same and that the α-subunit functions only to capture IL-2 via the pseudo-high-affinity complex. These results should prove useful not only in the design of IL-2-related therapeutics but also for the other cytokine receptors that share the IL-2Rγc subunit.

REFERENCES

1. Minami, Y., Kono, T., Miyazaki, T., and Taniguchi, T. (1993) *Annu. Rev. Immunol. 11*, 245.
2. Taniguchi, T., and Minami, Y. (1993) *Cell 73*, 5.
3. Sugamura, K., Asao, H., Kondo, M., Tanaka, N., Ishii, N., Nakamura, M., and Takeshita, T. (1995) *Adv. Immunol. 59*, 225.
4. Landgraf, B. E., Goldstein, B., Williams, D. P., Murphy, J. R., Sana, T. R., Smith, K. A., and Ciardelli, T. L. (1992) *J. Biol. Chem. 267*, 18511.
5. Wu, Z., Johnson, K. W., Goldstein, B., Choi, Y., Eaton, S., Laue, T. M., and Ciardelli, T. L. (1995) *J. Biol. Chem. 270*, 16039.
6. Myszka, D. G., Arulanantham, P. R., Sana, T., Wu, Z., Morton, T. A., and Ciardelli, T. L. (1996) *Protein Sci. 5*, 2468.
7. Russell, S. M., Johnston, J. A., Noguchi, M., Kawamura, M., Bacon, C. M., Friedmann, M., Berg, M., McVicar, D. W., Witthuhn, B. A., Silvennoinen, O., Goldman, A. S., Schmalsteig, F. C., Ihle, J. N., O'Shea, J. J., and Leonard, W. J. (1994) *Science 266*, 1042.
8. Nakamura, Y., Russell, S. M., Mess, S. A., Friedmann, M., Erdos, M., Francois, C., Jacques, Y., Adelstein, S., and Leonard, W. J. (1994) *Nature 369*, 330.
9. Wang, H. M., and Smith, K. A. (1987) *J. Exp. Med. 166*, 1055.
10. Teshigawara, K., Wang, H.-M., Kato, K., and Smith, K. A. (1987) *J. Exp. Med. 165*, 223.
11. He, Y.-W., and Malek, T. R. (1998) *Crit. Rev. Immunol. 18*, 503.
12. Williams, D. P., Regier, D., Akiyoshi, D., Genbauffer, F., and Murphy, J. R. (1988) *Nucleic Acids Res. 16*, 10453.
13. Sana, T. (1995) Ph.D. Thesis, Dartmouth Medical School, Hanover NH.
14. Sana, T., Wu, Z., Smith, K., and Ciardelli, T. (1994) *Biochemistry 33*, 5838.
15. Wu, Z., Johnson, K. W., Goldstein, B., Choi, Y., Eaton, S., Laue, T. M., and Ciardelli, T. L. (1995) *J. Biol. Chem. 270*, 16039.
16. Baker, D. P., Whitty, A., Zafari, M., R., Olson, D. L., Hession, C. A., Miatkowski, K., Avedissian, L. S., Foley, S. F., McKay, M. L., Benjamin, C. D., and Burkly, L. C. (1998) *Biochemistry 37*, 14337.
17. Myszka, D. G. (1999) *J. Mol. Recognit. 12*, 279.
18. Myszka, D. G., and Morton, T. A. (1998) *Trends Biochem. Sci. 23*, 149.
19. Myszka, D. G., and Morton, T. A. (1999) *CLAMP* (see www.cores.utah.edu/interaction).
20. Fisher, R., Fivash, M., Casas-Finet, J., Bladen, S., and McNitt, K. (1994) *Methods: Companion to Methods in Enzymology*, Academic Press, Vol. 6, pp 121.
21. Joss, L., Morton, T. A., Doyle, M. L., and Myszka, D. G. (1998) *Anal. Biochem. 261*, 203.
22. Wu, Z., Goldstein, B., Laue, T. M., Liparoto, S. F., Nemeth, M. J., and Ciardelli, T. L. (1999) *Protein Sci. 8*, 282.
23. Nelson, B. H., Lord, J. D., and Greenberg, P. D. (1994) *Nature 369*, 333.
24. Caligiuri, M., Zmuidzinas, A., Manley, T. J., Levine, H., Smith, K. A., and Ritz, J. (1990) *J. Exp. Med. 171*, 1509.
25. Chang, D. Z., Wu, Z., and Ciardelli, T. L. (1996) *J. Biol. Chem. 23*, 13349.
26. Johnson, K., Choi, Y., Wu, Z., Ciardelli, T., Granzow, R., Whalen, C., Sana, T., Pardee, G., Smith, K., and Creasey, A. (1994) *Eur. Cytokine Network 5*, 23.
27. Voss, S. D., Leary, T. P., Sondel, P. M., and Robb, R. J. (1993) *Proc. Natl. Acad. Sci. U.S.A. 90*, 2428.
28. Wu, Z., Johnson, K. W., Choi, Y., and Ciardelli, T. L. (1995) *J. Biol. Chem. 270*, 16045.
29. Liparoto, S. F., and Ciardelli, T. L. (1999) *J. Mol. Recognit. 12*, 316.
30. Lowenthal, J., and Greene, W. (1987) *J. Exp. Med. 166*, 1156.
31. Hemar, A., Subtil, A., Lieb, M., Morelon, E., Hellio, R., and Dautry-Varsat, A. (1995) *J. Cell Biol. 129*, 55.

BI011692M